Korean J. Chem. Eng., 34(6), 1748-1755 (2017)
DOI: 10.1007/s11814-017-0053-x

pISSN: 0256-1115
eISSN: 1975-7220

Ultrasonic-assisted leaching kinetics in aqueous $FeCl_3$-HCl solution for the recovery of copper by hydrometallurgy from poorly soluble chalcopyrite

Ho-Sung Yoon*, Chul-Joo Kim*, Kyung Woo Chung*, Jin-Young Lee*, Shun Myung Shin*, Sung-Rae Kim, Min-Ho Jang**, Jin-Ho Kim**, Se-Il Lee**, and Seung-Joon Yoo**,†**

*Korea Institute of Geoscience & Mineral Resources (KIGAM), 124 Gwahang-no, Yuseong-gu, Daejeon 34132, Korea
**Department of Biomolecular and Chemical Engineering, Seonam University, 7-111 Pyeongchon-gil, Songak, Asan 31556, Korea
(*Received 10 October 2016 • accepted 27 February 2017*)

Abstract−We studied the ultrasonic effect on the leaching of copper from poorly soluble chalcopyrite ($CuFeS_2$) mineral in aqueous $FeCl_3$ solution. The leaching experiment employed two methods, basic leaching and ultrasonic-assisted leaching, and was conducted under the optimized experimental conditions: a slurry density of 20 g/L in 0.1 M $FeCl_3$ reactant in a solution of 0.1 M HCl, with an agitation speed of 500 rpm and in the temperature range of 50 to 99 °C. The maximum yield obtained from the optimized basic leaching was 77%, and ultrasonic-assisted leaching increased the maximum copper recovery to 87% under the same conditions of basic leaching. In terms of the leaching mechanism, the overall reaction rate of basic leaching is determined by the diffusion of both the product and ash layers based on a shrinking core model with a constant spherical particle; however, in the case of ultrasonic-assisted leaching, the leaching rate is determined by diffusion of the ash layer only by the removal of sulfur adsorbed on the surface of chalcopyrite mineral.

Keywords: Leaching Kinetics, Poorly Soluble Chalcopyrite Mineral, Basic Leaching, Ultrasonic-assisted Leaching, Ferric Chloride, Shrinking Core Model, Product and Ash Layer Diffusion, Ash Layer Diffusion

INTRODUCTION

Copper minerals occur in various chemical forms such as sulfides, oxides, carbonates, and hydroxides, as shown in Table 1. Among them, the most abundant copper-containing mineral is known to be chalcopyrite, which constitutes about 70% of copper minerals in total [1].

Most of the copper in high-grade chalcopyrite is generally recovered by a pyrometallurgical process, at which time SO_2 is produced during the roasting process. This requires the SO_2 gas to be captured and converted into sulfuric acid to prevent air pollution. Accordingly, this pyrometallurgical process contributes to increasing the cost of operating the plant. Thus, the hydrometallurgical process, which has become a viable alternative to the pyrometallurgical process, is capable of selectively leaching the metal component, and more importantly it can be used to treat low-grade minerals at a relatively lower cost [2].

Table 1. Various types of copper minerals

Mineral	Types	Species
Copper minerals	Sulfide minerals	Chalcopyrite, $CuFeS_2$
		Chalcocite, Cu_2S
		Bornite, $2Cu_2S{\cdot}CuS{\cdot}FeS$
		Covellite, CuS
		Digenite, Cu_9S_5
	Oxide minerals	Cuprite, Cu_2O
		Chrysocolla, CuO
	Carbonate minerals	Malachite, $CuCO_3{\cdot}Cu(OH)_2$
		Azurite, 2 $CuCO_3{\cdot}Cu(OH)_2$
	Hydroxide mineral	Atacamite, $Cu_2(OH)_3Cl$

Leaching is the most important process in the overall hydrometallurgical process. Generally, it is carried out by adding an appropriate oxidant to the solution. In this study, we selected ferric chloride as an appropriately strong and inexpensive oxidant from among the various oxidants that are available. The leaching reaction of chalcopyrite in an aqueous solution of ferric chloride is expressed by Eq. (1), which shows solid sulfur to be the major product of the reaction.

$$CuFeS_2+4FeCl_3 \leftrightarrow CuCl_2+5FeCl_2+2S^0 \quad (1)$$

This sulfur is adsorbed on the surface of unreacted mineral where it forms a layer. The layer, which acts as a barrier against the leaching, is commonly known as a passivation layer. This layer is the main form of resistance against the penetration of oxidant into the chalcopyrite mineral [1-8].

Generally, chalcopyrite is a poorly soluble mineral ore because it takes a long time, more than one month, for leaching. If it is a lower grade mineral, an even longer leaching time is required. This long leaching time hinders the commercial application of the hydrometallurgical process. Therefore, we investigated the possibility of using the ultrasonic effect to improve the yield and reaction rate of the leaching process of copper from poorly soluble chalcopyrite.

†To whom correspondence should be addressed.
E-mail: sjyoo001@hanmail.net

Table 2. Summary of hydrometallurgical process of chalcopyrite with various oxidants

No.	Oxidants	Mechanism	Activation energy (kJ/mol)	Yield (%)	Condition	Ref.
1	$Fe_2(SO_4)_3$-NaCl	Chemical reaction and diffusion control	-	45-91	95 °C, 5.5 μm	8
2	$FeCl_3$-HCl	Chemical reaction	55±5	<16	3.5-80 °C −315+200 μm	9
3	$FeCl_3$-CCl_4	Diffusion control	31.2	35	45-80 °C <100 μm	10
	$FeCl_3$	Diffusion/ Chemical reaction	1.1/69	<16	2.5-45 °C/45-80 °C <100 μm	
4	$FeCl_3$-$CuCl_2$	Chemical reaction	69	<35	70-90 °C, <38 μm	11
5	$CuCl_2$-NaCl	Diffusion control	71	63	75-104 °C, 56-71 μm	12
6	$CuCl_2$-NaCl	-	-	38.3	80-100 °C, <200 μm	13
7	HCl-$CuCl_2$-NaCl	Electrochemical oxidation	59.5	-	60-90 °C, 0.3-0.5 cm^2 Disk	14
8	$K_2Cr_2O_7$	Diffusion control	24	>80	50-97 °C, 75 μm	15
9	H_2O_2-H_2SO_4	Surface reaction	60	<60	25-60 °C, 40-80 μm	16
10	MnO_2-HCl	-	-	<70	20-70 °C, <200 μm	17
10	NH_4I-I_2	Reaction control	50 30.3	-	16-35 °C, 35-60 °C, 1.7 cm	18

1. Basic Leaching

In the basic leaching process, copper is reacted with $FeCl_3$ as the reactant in an aqueous solution of HCl. The reaction is represented by Eq. (1). The solid sulfur (S^o) produced from the reaction is adsorbed and distributed over the surface of the chalcopyrite mineral particles.

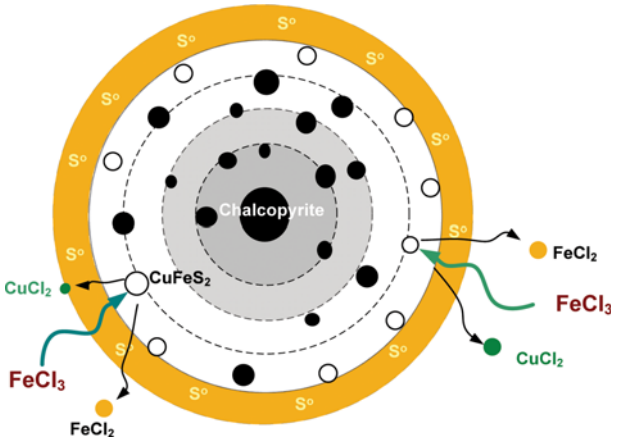

Fig. 1. Schematic diagram depicting the leaching behavior of chalcopyrite during basic leaching.

Many oxidants have been used effectively for the leaching process as shown in Table 2. The main leaching mechanism and activation energy according to the type of oxidants are summarized in Table 2.

Fig. 1 shows an illustration of the mechanism of basic leaching. The copper component is oxidized by $FeCl_3$ in an environment of aqueous HCl to produce $CuCl_2$ as the product and the $FeCl_2$ and S^o components as side products.

In this study, we investigated the effect of the process variables to determine the optimal conditions of basic leaching.

2. Ultrasonic-assisted Leaching

The solid sulfur powder produced during the reaction is adsorbed on the surface of the chalcopyrite mineral and then forms an outer surface layer as shown in Fig. 1. The layer acts as a resistance barrier against the penetration of the $FeCl_3$ oxidant into the interior of mineral particles. Many researchers consider this layer as a passivation layer [1-8].

In this study, ultrasonic vibration was applied to the reactor to disperse the sulfur powder adsorbed on the surface of the chalcopyrite mineral into the solution, as shown in Fig. 2. Although, some similar studies [19-22] involving ultrasonic input have been done, the leaching kinetics and mechanism of reactions have not yet

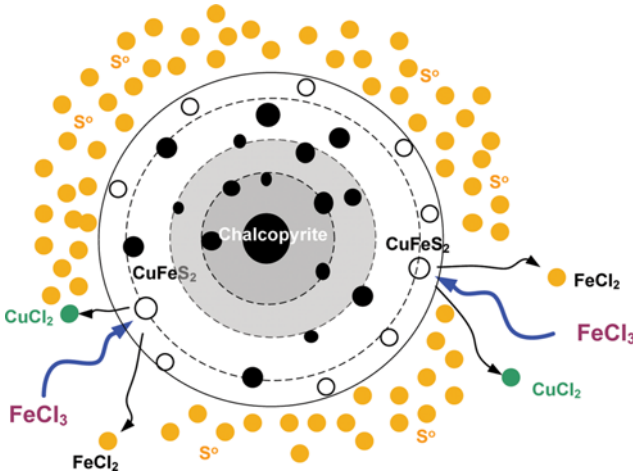

Fig. 2. Schematic diagram representing the leaching behavior of chalcopyrite during ultrasonic-assisted leaching.

been studied definitively.

EXPERIMENTAL

1. Materials and Procedure

Chalcopyrite ($CuFeS_2$) mineral that was used as a raw material was obtained from LS-Nikko Copper Metallurgy in Korea. The particle size of the chalcopyrite mineral used in our experiment was in the range of 3-25 μm with a median size of 15 μm. Ferric chloride as a leaching agent was selected as an appropriately strong oxidant and inexpensive reactant from among the available oxidants such as $Fe_2(SO_4)_3$ [8], $FeCl_3$ [9-11], $CuCl_2$ [12-14], $K_2Cr_2O_7$ [15], H_2O_2 [16], MnO_2 [17], and NH_4I [18].

The leaching experiment involved a slurry density of 20 g $CuFeS_2$/L, 0.1 M $FeCl_3$, and the experimental conditions were agitation at 500 rpm in the temperature range of 50 to 99 °C using the Pyrex reactor shown in Fig. 3. Here the 0.1 M $FeCl_3$ corresponds to the stoichiometric ratio for the initial amount of copper existing in the chalcopyrite mineral measured from ICP-MS. The HCl concentration was in the range of 0.02 M to 0.5 M HCl, and 0.1 M HCl was selected as the optimized condition for the maximum yield of copper recovery. Reaction temperature was difficult to carry out the condition less than 50 °C because of self-exothermic heat of ultrasonic probe. Accordingly, the range of leaching temperature was selected by the condition of 50 to 99 °C.

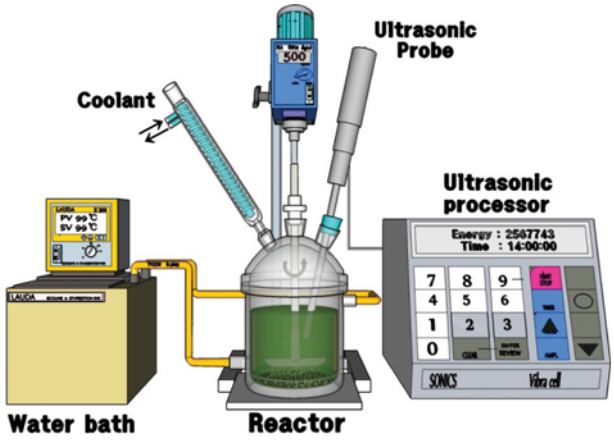

Fig. 3. Schematic diagram of experimental apparatus for ultrasonic-assisted leaching.

Ultrasonic effect was investigated at the condition of constant ultrasound input with a low intensity. Ultrasound was constantly inputted to the solution using a tip-type standard probe (13 mm in diameter and 136 mm in length) by using an ultrasonic processor (VC 750 model, Sonics & Materials Inc. USA). The ultrasonic power with a low intensity of 5 W was directly delivered into the leaching solution.

2. Measurements

The metal composition of the chalcopyrite was analyzed by inductively coupled plasma-mass spectrometry (ICP-MS, X-series (X5), Thermo Elemental, UK) with high sensitivity and accuracy because ICP-MS also allows rapid simultaneous multi-element determination [28].

The pH values were measured by using the pH electrode of an advanced electrochemistry meter (Orion VERSASTAR, Thermo Scientific).

The morphology of the particles before and after the leaching process was observed by scanning electron microscope (15 kV, JEOL, JSM-6400). The sample that was used for the SEM investigation was first washed with a sufficient amount of water.

Copper solution, which was removed periodically from the reaction vessel for analysis, was filtered by a syringe filter with 0.2 μm pores, and then the copper ion concentration was analyzed by inductively coupled plasma-atomic emission spectrometry (ICP-AES, *i*CAP6000, Thermo Fisher, UK). The wavelength for ICP-AES analysis was selected as 430.3 nm, at which interference between the elements is minimized.

Nitrogen adsorption and desorption was measured at 77 K using a Micromeritics TriStar 3000 automatic analyzer after the sample was degassed for 2 h in the degas port of the adsorption apparatus.

RESULTS AND DISCUSSION

In this study, the leaching of poorly soluble chalcopyrite was hypothesized by using a spherical shrinking-core model with a constant size. The first step in the reaction mechanism is the diffusion of the product layer because the solid sulfur powder produced through the leaching reaction is adsorbed and distributed on the surface of the ore mineral. The next step of the reaction mechanism is determined by diffusion through the ash layer by gangue that remained unreacted during the leaching process.

Ultimately, the total leaching mechanism was assumed to be determined by two layers, the product layer and the ash layer, as shown in Fig. 1. Assuming this diffusion model consisting of product and ash layers is based on the spherical shrinking core model [23-27] with a constant particle size Eq. (2).

$$1-3(1-X_B)^{2/3}+2(1-X_B)=k_{P\&A}t \text{ or } k_At \quad (2)$$

where $k_{P\&A}$ is the apparent rate constant for the diffusion of the product and ash layers in basic leaching, k_A is the apparent rate con-

Table 3. Elemental composition of chalcopyrite analyzed by ICP-MS

Comp.	Fe %	Cu %	Na %	K %	Ca %	Co mg/kg	Zn mg/kg	Mo mg/kg	Ni mg/kg	Ag mg/kg	Au mg/kg
$CuFeS_2$	20.3	41.5	0.15	0.31	0.52	21	745	473	3	44	<1

Table 4. Physical properties of chalcopyrite before and after leaching

Characteristics	Unit	Raw mineral	After basic leaching	After ultrasonic-assisted leaching
Surface area (BET)	m^2/g	4	16	10
Pore volume	cm^3/g	0.013	0.09	0.05
Average pore size	nm	11	23	20

stant for the diffusion of the ash layer only in ultrasonic-assisted leaching and is inversely related to the time required for complete conversion of a particle, r_c=0.

$$k_{P\&A} \text{ or } k_A = \frac{2D_e C_{Ao}}{\rho_B R^2}$$

Table 3 presents the elemental composition of chalcopyrite analyzed by ICP-MS to measure the chemical components included in the chalcopyrite. The result of the analysis showed that the copper content of the chalcopyrite was 41.5%, as shown in Table 2. The mineral was mainly found to be composed of Cu, Fe and metals of low atomic numbers such as Na, K, Ca, Zn, Mo and numerous minor constituents such as Co and Ag.

The leaching of copper was carried out under the following conditions: a slurry density of 20.0 g $CuFeS_2$/L, agitation of 500 rpm in a temperature range of 50 to 99 °C. In HCl medium, the copper component in $CuFeS_2$ is converted to cupric chloride ($CuCl_2$) by ferric chloride ($FeCl_3$).

The advantage of leaching by using a hydrochloric acid medium is that it is generally faster than a sulfate medium, and it can react at a higher pulp density. Furthermore, the copper product is recovered in the form of $CuCl_2$, which is easier to transform to other copper compounds. Apparently, no information has been published on the definite behavior of chalcopyrite in the presence of HCl since the previous report [29], but Havlik and Kammel proposed that the HCl is added to prevent iron hydrolysis in the leaching of chalcopyrite [10]. Recent researches [1,2] have reported that the addition of chloride and H^+ ions has a positive effect on the leaching rate of chalcopyrite in the presence of an oxidant.

The result of N_2 adsorption and desorption revealed the BET surface area of the mineral to have values of 4.4 m^2/g before leaching in the case of the chalcopyrite mineral, and 16 m^2/g after basic leaching at 99 °C for 14 h. On the other hand, the value of the surface area was determined to be 10 m^2/g after ultrasonic-assisted leaching, as shown in Table 4. The copper is leached out by the $FeCl_3$ oxidant during basic leaching and the sites retain the macropores. Furthermore, the sulfur powder was adsorbed on the sites thereby sharply increasing the BET surface area to 16 m^2/g.

In the case of ultrasonic-assisted leaching, however, desorption of the adsorbed sulfur powder by ultrasonic vibration sharply decreased the BET surface area from 16 m^2/g to 10 m^2/g.

The N_2 adsorption-desorption isotherms of chalcopyrite and the pore size distribution before and after basic leaching are plotted in Fig. 4. The average pore size and pore volume were calculated by the BJH method. After basic leaching, pore size distribution and hysteresis were newly shown by pore formation, with an average pore size of 23 nm and pore volume of 0.09 cm^3/g. On the other hand, ultrasonic-assisted leaching resulted in an average pore diameter of 20 nm and pore volume of 0.05 cm^3/g.

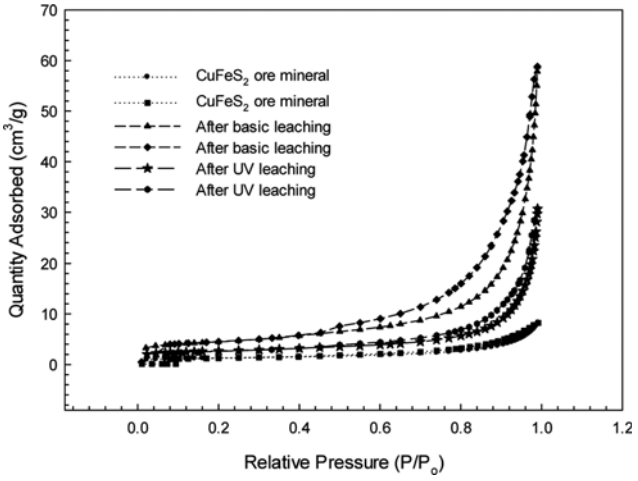

Fig. 4. N_2 gas adsorption and desorption isotherms of chalcopyrite before and after basic and ultrasonic-assisted leaching.

During basic leaching, the mineral particles were assumed to have a constant size within a range. This is because the sulfur powder produced by the reaction is initially adsorbed on the surface of the mineral, which additionally acts as a barrier against leaching. Eventually, the final overall extent to which this layer obstructs leaching is affected by the diffusion of the product and ash layers during basic leaching.

However, in the case of ultrasonic-assisted leaching, the rate-determining step was assumed to be the diffusion of the ash layer only, because the adsorbed sulfur layer is dispersed into the solution and the product layer disappears from the surface of the mineral. Finally, the particle size was reduced as the product layer formed but the difference was not large and was of the order of 5 μm. The particle size was assumed to be constant before and after leaching.

Fig. 5 shows the adsorption/desorption isotherms and pore size distributions before and after basic and ultrasonic-assisted leach-

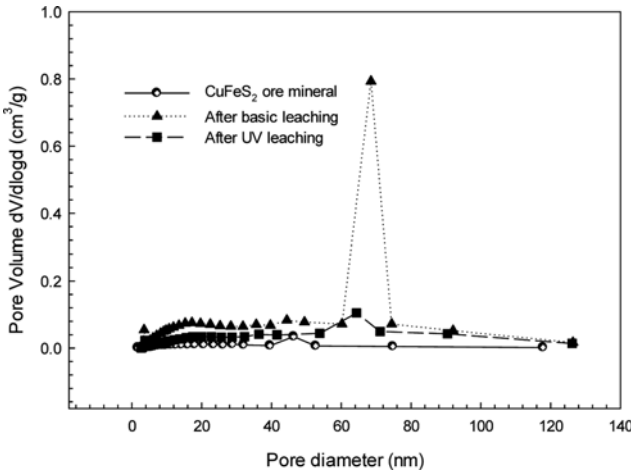

Fig. 5. Pore size distribution before and after basic leaching and ultrasonic-assisted leaching.

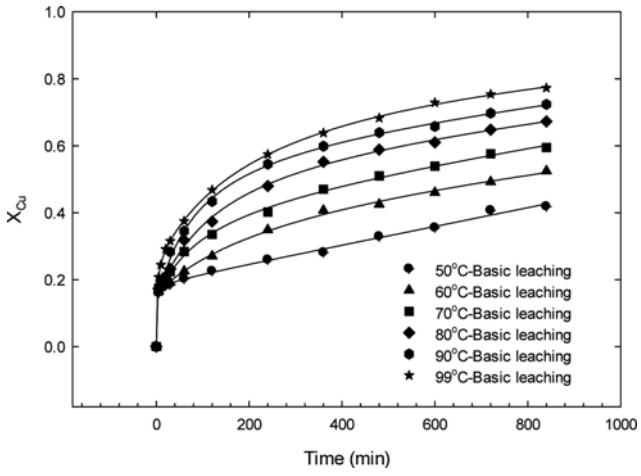

Fig. 7. Fractional conversion during the evolution of copper in basic leaching.

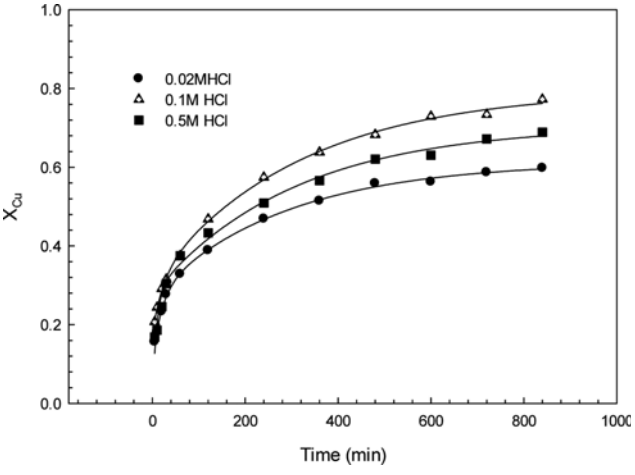

Fig. 6. Influence of the concentration of acid on chalcopyrite leaching at 99 °C.

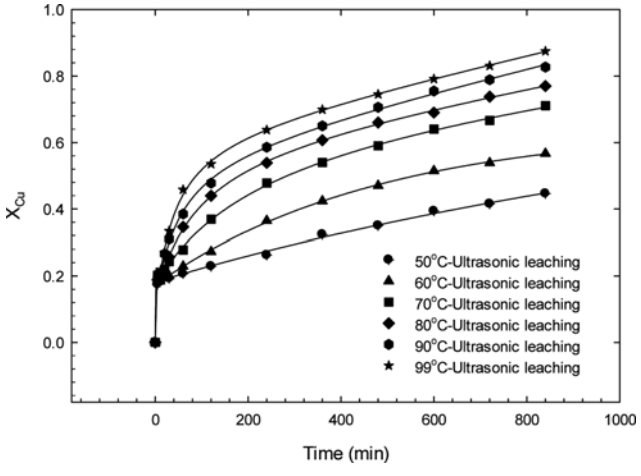

Fig. 8. Fractional conversion during the evolution of copper in ultrasonic-assisted leaching.

ing. Initially, the raw mineral had no pore but basic leaching resulted in the formation of macropores of 60 to 80 nm diameter in the chalcopyrite.

In the case of ultrasonic-assisted leaching, the rough surface of the mineral was peeled off into the solution as small fragments by the mechanical shock of ultrasonic vibration. Thus, the pore size was gradually reduced, as shown in Fig. 5. In summary, basic leaching transformed the mineral into a porous state, whereas ultrasonic-assisted leaching mostly caused the macropores to disappear, as shown in Fig. 5.

Fig. 6 represents the fractional conversion of copper according to the HCl concentration. The optimal HCl condition was found by varying the concentration in the range 0.02 M to 0.5 M HCl for a fixed concentration of 0.1 M $FeCl_3$ at 99 °C. The experimental results showed that the highest yield of copper was obtained at 0.1 M HCl; hence, thereafter the concentration of HCl was maintained at 0.1 M based on the experimental result.

Fig. 7 shows the fractional conversion of copper at various tem-

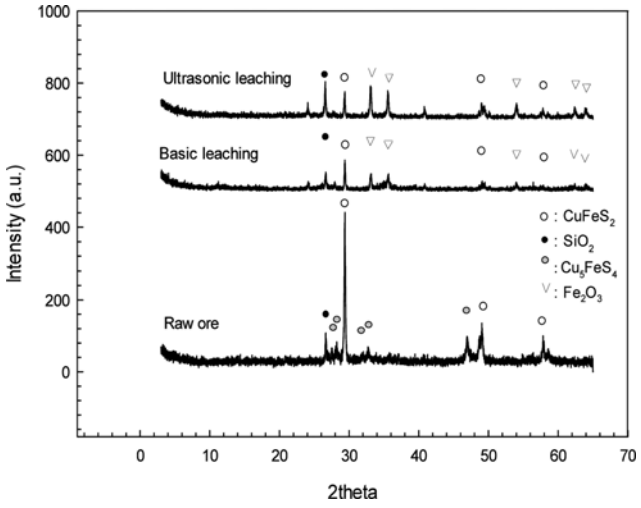

Fig. 9. Comparison of crystalline peaks according to leaching methods.

peratures during basic leaching. Each temperature curve increased exponentially as a function of time, as shown in the figure. The maximum yield that was obtained was 77% after basic leaching for 14 h under the conditions of 0.1 M $FeCl_3$, 0.1 M HCl, and 99 °C.

On the other hand, Fig. 8 shows the fractional conversion of copper at various temperatures during ultrasonic-assisted leaching. This time, the maximum yield was increased to 87% after ultrasonic-assisted leaching for 14 h under the conditions 0.1 M $FeCl_3$, 0.1 M HCl, and 99 °C.

As shown in Fig. 9, the main crystalline peak corresponding to the crystallinity of chalcopyrite is indicated at 29.4° on the XRD pattern [30]. The peak decreased sharply after the leaching process. More specifically, in the case of ultrasonic-assisted leaching, the intensity of the peak was considerably reduced and peaks corresponding to the crystalline structure of Fe_2O_3 were found to have shifted to higher 2θ values than after basic leaching. As indicated, ultrasonic-assisted leaching is more effective than basic leaching because Fe_2O_3 is produced because of the reaction of the Fe component in the chalcopyrite.

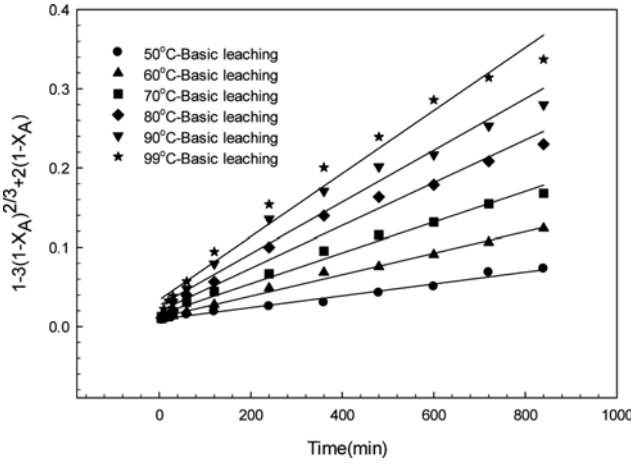

Fig. 10. Kinetic constants obtained from diffusion model equation during basic leaching.

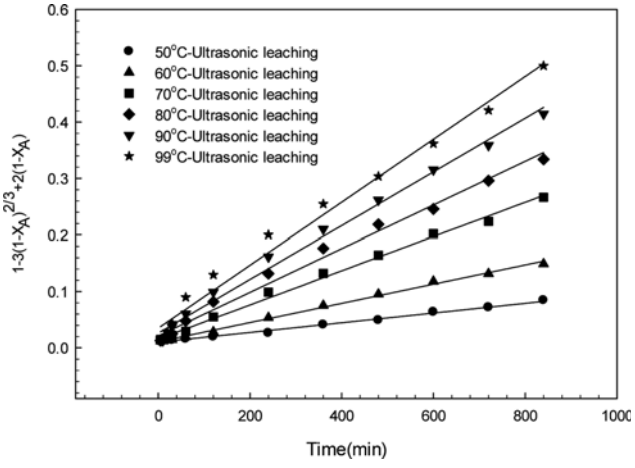

Fig. 11. Kinetic constants obtained from ash layer diffusion model equation during ultrasonic-assisted leaching.

In basic leaching, the rate equation can be summarized as in Eq. (2) for the product and ash layers using the shrinking core model that has the shape of a constant spherical particle. Based on Eq. (2), the apparent rate constant ($k_{p\acute{e}a}$) was fitted by using data

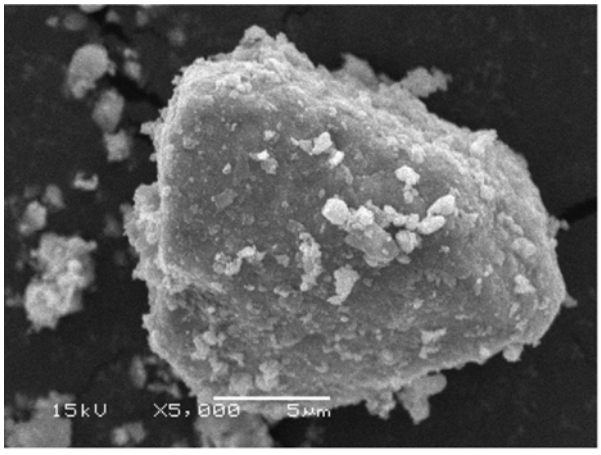

(a)

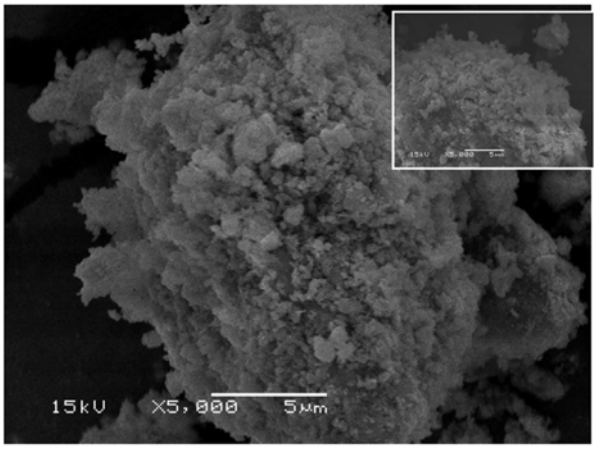

(b)

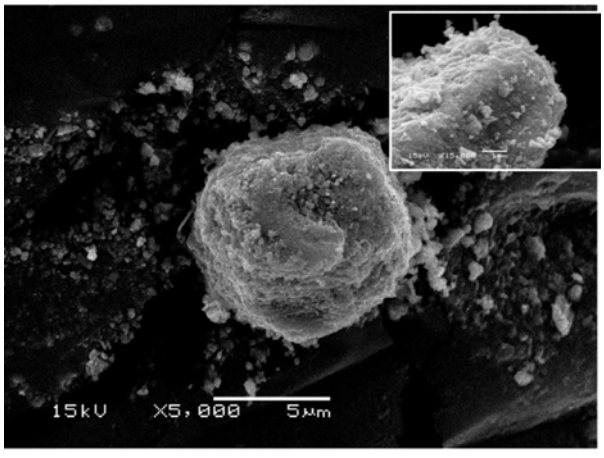

(c)

Fig. 12. SEM photographs of chalcopyrite before and after basic and ultrasonic-assisted leaching at 99 °C for 14 h: (a) Raw mineral (b) Residue of basic leaching (c) Residue of ultrasonic-assisted leaching.

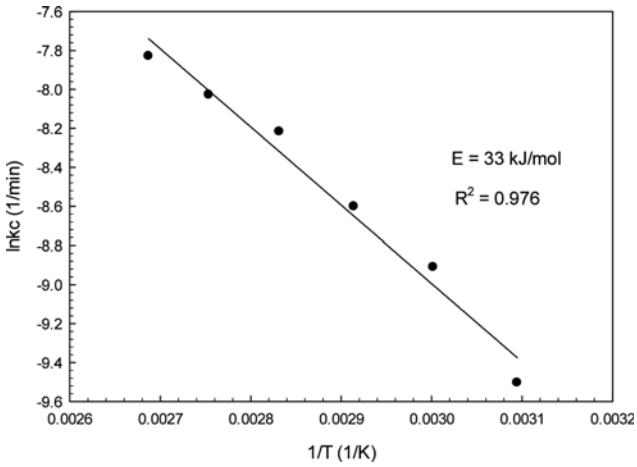

Fig. 13. Arrhenius plot obtained from basic leaching.

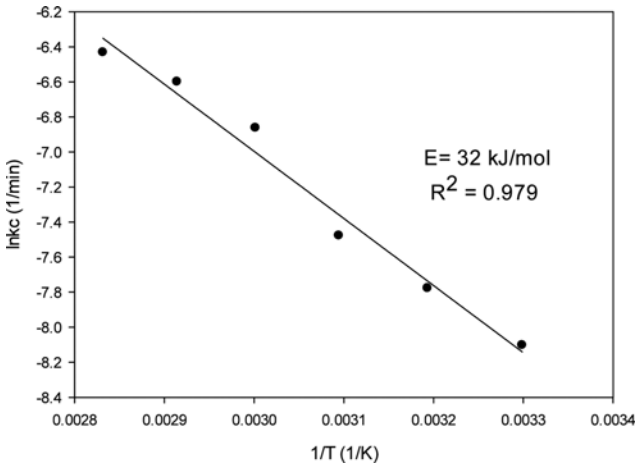

Fig. 14. Arrhenius plot obtained for ultrasonic-assisted leaching.

obtained at various temperatures as shown in Fig. 10.

In the case of ultrasonic-assisted leaching, the rate equation was applied to the same model as expressed by Eq. (2) even though it was only applied to the diffusion of the ash layer contrary to basic leaching. Based on Eq. (2), the least-squares method was used to calculate the apparent rate constant (k_a) from the fitted data at various temperatures as shown in Fig. 11.

The raw mineral had a median particle size of about 15 μm, as shown in Fig. 12(a), and particles retained this size after basic leaching, as shown in Fig. 12(b), because the surface of the mineral was covered in fine sulfur powder produced through the leaching reaction. Finally, the overall particle size was not noticeably changed by basic leaching in comparison to that of the initial mineral, whereas it was partly decreased to the scale of 10 μm by ultrasonic-assisted leaching, as shown in Fig. 12(c). The reason is that the sulfur powder adsorbed on the surface of the mineral is dispersed from the surface into the solution due to ultrasonic vibration.

The dissolution kinetics of basic leaching can be represented by the shrinking-core model with a diffusion mechanism through product and ash layers as the rate-controlling step and the slope could be obtained as -4.013×10^3 as shown in Fig. 13. The slope was used to calculate the apparent activation energy as 33 kJ/mol in the range of 50 to 99 °C.

In the case of ultrasonic-assisted leaching, the slope was -3.830×10^3 as shown in Fig. 14 and the apparent activation energy was found to be 32 $kJmol^{-1}$ for the same temperature range.

Table 5 summarizes the experimental results obtained from basic and ultrasonic-assisted leaching. Although the rate constants were of the same order in all the cases, that of ultrasonic-assisted leaching was shown to be higher than basic leaching because it is affected by the ash layer diffusion as the only difference from basic leaching.

On the other hand, the apparent activation energies had low values caused by the diffusion mechanism of the two different leaching processes. Both the leaching processes were ultimately found to be insensitive to temperature.

CONCLUSIONS

This paper presents an investigation of the effect of applying ultrasonic vibration to the leaching of copper from poorly soluble chalcopyrite mineral. In the case of basic leaching, the overall reaction rate was determined by the diffusion of two layers with a layer of solid sulfur produced during leaching and an ash layer remaining after leaching. This procedure yielded 77% copper with an apparent activation energy of 33 kJ/mol in the range of 50 to 99 °C.

On the other hand, in the case of ultrasonic-assisted leaching, the overall reaction rate was only determined by the diffusion of the ash layer without sulfur layer, because the sulfur layer is removed from the surface by ultrasound.

Table 5. Kinetic results of basic leaching and ultrasonic-assisted leaching

Basic leaching	$FeCl_3$ conc. (mol/L)	HCl conc. (mol/L)	Product and ash layer diffusion step						Activation energy (kJ/mol)	Yield	Cond.
			$k_{p\&A}$ (1/min)×10^{-4}								
			50 °C	60 °C	70 °C	80 °C	90 °C	99 °C			
	0.1	0.1	0.75	1.349	2.35	2.70	3.26	3.98	33	77	20 g/L, 500 rpm
Ultrasonic-assisted leaching	$FeCl_3$ conc. (mol/L)	HCl conc. (mol/L)	Ash layer diffusion step						Activation energy (kJ/mol)	Yield	Cond.
			k_A (1/min)×10^{-4}								
			50 °C	60 °C	70 °C	80 °C	90 °C	99 °C			
	0.1	0.1	0.86	1.70	3.03	3.87	4.76	5.58	32	87	20 g/L, 500 rpm

Finally, ultrasonic-assisted leaching highly increased the yield to 87% in spite of poorly soluble chalcopyrite. In the case of activation energy, it had a value of 32 kJ/mol because the leaching mechanism was applied by the same diffusion model like the basic leaching. The apparent activation energy showed at the value of 32 kJ/mol because it is easy for $FeCl_3$ oxidant to penetrate the core of chalcopyrite by the removal of sulfur layer than the basic leaching with 33 kJ/mol.

In conclusion, the leaching efficiency could be increased to 10% than the basic leaching by adding the ultrasonic device easily and simply to the reactor despite the poorly soluble sulfide mineral.

NOMENCLATURE

C_A : concentration of chalcopyrite reactant [$molL^{-1}$]
C_A : concentration of $FeCl_3$ reactant [$molL^{-1}$]
C_{A0} : initial concentration of $FeCl_3$ reactant [$molL^{-1}$]
C_B : concentration of chalcopyrite reactant [$molL^{-1}$]
C_{B0} : initial concentration of chalcopyrite reactant [$molL^{-1}$]
D_e : is the effective diffusion coefficient of the $FeCl_3$ oxidant through the product and ash layers
$E_{p\&A}$: apparent activation energy for product and ash layer diffusion in basic leaching [$kJmol^{-1}$]
E_A : apparent activation energy for ash layer diffusion in ultrasonic-assisted leaching [$kJmol^{-1}$]
$k_{p\&A}$: first-order rate constant for product and ash layer diffusion in basic leaching [s^{-1}]
k_A : apparent rate constant for ash layer diffusion in ultrasonic-assisted leaching [s^{-1}]
N_A : moles of $FeCl_3$ reactant [mol]
N_B : moles of chalcopyrite reactant [mol]
N_{B0} : vinitial moles of chalcopyrite reactant [mol]
r_c : radius of unreacted chalcopyrite [m]
R : radius of the initial chalcopyrite particle [m]
S_{ex} : external surface area [m^2]
t : time [s]
T : temperature [K]
X_A : fraction of converted $FeCl_3$
X_B : fraction of converted copper in chalcopyrite

Greek Letter

ρ_B : molar density of copper component included in chalcopyrite [$molL^{-1}$]

ACKNOWLEDGEMENT

The research was supported by the Basic Research Project of the Korea Institute of Geoscience and Mineral Resources (KIGAM) funded by the Minister of Science, ICT and Future Planning of Korea.

REFERENCES

1. Y. Li, N. Kawashima, J. Li, A. P. Chandra and A. R. Gerson, *Adv. Colloid Interface Sci.*, **197**, 1 (2013).
2. Y. J. Xian, S. M. Wen, J. S. Deng, J. Liu and Q. Nie, *Canadian Metallurgical Quarterly*, **51**, 133 (2012).
3. R. P. Hackl, D. B. Dreisinger, E. Peters and J. A. King, *Hydrometallurgy*, **39**, 25 (1995).
4. E. M. Cordoba, J. A. Munoz, M. L. Blazquez, F. Gonzalez and A. Ballester, *Minerals Engineering*, **22**, 229 (2009).
5. M. B. Stott, H. R. Watling, P. D. Franzmann and D. Sutton, *Minerals Engineering*, **13**, 1117 (2000).
6. A. Parker, C. Klauber, A. Kougianos, H. R. Watling and W. van Bronswijk, *Hydrometallurgy*, **71**, 265 (2003).
7. G. Viramontes-Gamboa, M. M. Pena-Gomar and D. G. Dixon, *Hydrometallurgy*, **105**, 140 (2010).
8. M. F. C. Carneiro and V. A. Leao, *Hydrometallurgy*, **87**, 73 (2007).
9. T. Havlik, M. Skrobian, P. Balaz and R. Kammel, *Int. J. Miner. Process.*, **43**, 61 (1995).
10. T. Havlik and R. Kammel, *Minerals Engineering*, **8**, 1125 (1995).
11. M. Al-Harahsheh, S. Kingman and A. Al-Harahsheh, *Hydrometallurgy*, **91**, 89 (2008).
12. M. Bonan, J. M. Demarthe, H. Renon and F. Baratin, *Metallurgical Transactions B*, **12B**, 269 (1981).
13. M. Skrobian, T. Havlik and M. Ukasik, *Hydrometallurgy*, **77**, 109 (2005).
14. T. Hirato, H. Majima and Y. Awakura, *Metallurgical Transactions B*, **18B**, 31 (1987).
15. S. Aydogan, G. Ucar and M. Canbazoglu, *Hydrometallurgy*, **81**, 45 (2006).
16. M. M. Antonijevic, Z. D. Jankovic and M. D. Dimitrijevic, *Hydrometallurgy*, **71**, 329 (2004).
17. T. Havlik, M. Laubertova, A. Miskufova, J. Kondas and F. Vranka, *Hydrometallurgy*, **77**, 51 (2005).
18. Y. C. Guan and K. N. Han, *Metallurgical and Material Transactions B*, **28B**, 979 (1997).
19. X. Juanqin, L. Xi, D. Yewei, M. Weibo, W. Yujie and L. Jingxian, *Chinese J. Chem. Eng.*, **18**, 948 (2010).
20. S. G. Chen, *Sanghai Nonferrous Metals*, **3**, 142 (2003).
21. R. N. Kar, L. B. Sulka and K. M. Swamy, *Metallurgical and Materials Transactions B*, **27**, 351 (1996).
22. B. Pesic and T. L. Zhou, *Metallurgical Transactions B*, **23B**, 13 (1992).
23. O. Levenspiel, *Chemical Reaction Engineering*, 3rd Ed., Wiley, NewYork (2003).
24. L. D. Schmidt, *The Engineering of Chemical Reactions*, 2nd Ed., Oxford University Press (2005).
25. M. Avrami, *J. Chem. Phys.*, **7**, 1103 (1939).
26. C. F. Dickinson and G. R. Heal, *Thermochim. Acta*, **340**, 89 (1999).
27. J. J. M. Órfão and F. G. Martins, *Thermochim. Acta*, **390**, 195 (2002).
28. T. N. Akinlua and T. R. Ajayi, *Fuel*, **87**, 1469 (2008).
29. M. L. O'Malley and K. C. Liddell, *Metallurgical Transactions B*, **18B**, 505 (1987).
30. D. Maurice and J. A. Hawk, *Hydrometallurgy*, **51**, 371 (1999).